Published in JOURNAL OF MICROMECHANICS AND MICROENGINEERING
22, 2, 025013 (8pp), 2012
which should be used for any reference to this work

Microfabricated rubidium vapour cell with a thick glass core for small-scale atomic clock applications

Y Pétremand[1], C Affolderbach[2], R Straessle[1], M Pellaton[2], D Briand[1], G Mileti[2] and N F de Rooij[1]

[1] Ecole Polytechnique Fédérale de Lausanne (EPFL), Institute of Microengineering (IMT), Sensors, Actuators and Microsystems Laboratory, Rue Jaquet-Droz 1, 2000 Neuchâtel, Switzerland
[2] Laboratoire Temps-Fréquence (LTF), Université de Neuchâtel, 2000 Neuchâtel, Switzerland

E-mail: yves.petremand@epfl.ch

Abstract
This paper presents a new fabrication method to manufacture alkali reference cells having dimensions larger than standard micromachined cells and smaller than glass-blown ones, for use in compact atomic devices such as vapour-cell atomic clocks or magnetometers. The technology is based on anodic bonding of silicon and relatively thick glass wafers and fills a gap in cell sizes and technologies available up to now: on one side, microfabrication technologies with typical dimensions $\leqslant 2$ mm and on the other side, classical glass-blowing technologies for typical dimensions of about 6–10 mm or larger. The fabrication process is described for cells containing atomic Rb and spectroscopic measurements (optical absorption spectrum and double resonance) are reported. The analysis of the bonding strength of our cells was performed and shows that the first anodic bonding steps exhibit higher bonding strengths than the later ones. The spectroscopic results show a good quality of the cells. From the double-resonance signals, we predict a clock stability of $\approx 3 \times 10^{-11}$ at 1 s of integration time, which compares well to the performance of compact commercial Rb atomic clocks.

(Some figures may appear in colour only in the online journal)

1. Introduction

Vapour-cell atomic clocks (‘Rb clocks’) [1] are the most compact realizations of atomic clocks [2] and serve as precise frequency and time references in numerous applications such as telecommunication, network synchronization or satellite navigation, with several thousands of units sold every year. Effort has been made and is still being made towards the miniaturization of vapour-cell atomic clocks [3] in view of emerging applications in mobile and low-power instrumentation or end-user devices. This miniaturization has many advantages (e.g. reducing the power consumption, the mass and the production cost of the clock’s physics package) but a drawback is that it degrades the short-term stability (expressed in terms of the Allan deviation) [4] when the size of the alkali vapour cell used in the clock is reduced [5]. Previously reported chip-scale devices were manufactured using MEMS (microelectromechanicalsystems) microfabrication processes and anodic bonding [3, 6–11]. These devices show a typical optical path length from a couple of hundreds of microns up to about 1.5 mm. For higher precision clocks—and practically all commercially available cell clocks—glass-blown cells are generally used but this technique is limited to cell volumes bigger than few tens of cubic millimetres (characteristic size of 6–10 mm) [12–14].

Here we present a technology that fills the gap in achievable cell sizes between the chip-scale MEMS cells and the more macroscopic glass-blown cell bodies. For applications where a cell size with critical internal dimensions of few millimetres is required, the glass-blown technique does not allow good control of cell geometry or flat window surfaces [12, 13], and standard MEMS technology based on DRIE (deep reactive ion etching) or KOH etching of silicon is not applicable due to the required etching depth. Our

technology allows producing cells with few millimetres of typical size, while providing excellent control of cell geometry and window quality, tight cell sealing and highly parallel production of many cells at a time. Although such cells do not aim for ultimate miniaturization of the clock, they are of great importance for the realization of highly compact commercial vapour-cell clocks—either based on the coherent population trapping (CPT) [3, 15] or double-resonance (DR) approach [16].

2. Alkali cell fabrication technologies

In this section, we discuss the main advantages and disadvantages of the state-of-the-art cell fabrication techniques, depending on the application or the requirements.

2.1. Glass-blowing technique

The glass-blowing technique, discovered around 50 B.C. [17], is still used today. It consists in creating an object by gathering molten glass at the end of a hollow blowing pipe and inflating it like a bubble. It can be blown into a hollow mould to form it with good precision or freely shaped with simple tools. Modern variants of this technique for soldering glass to glass also make use of precision machining and highly reproducible glass preforms, and are used as state-of-the-art technology for the fabrication of macroscopic alkali cells for commercially available vapour-cell atomic clocks. It is possible to obtain cells exempt of impurities, and long cell lifetimes were already proven, e.g. by commercial Rb clocks. The inconvenience of this technology appears when reducing the size of the cell drastically down to a couple of millimetres: the soldering of glass by melting it induces rounded edges and makes it very difficult to precisely meet the desired cell geometry. Furthermore, the melting of the glass prevents obtaining a flat window surface quality at these small dimensions, which results in undesirable intensity losses for the light sent through the cell for clock operation. The minimal achievable cell size with reasonably acceptable quality is of around 6–10 mm total length or diameter for this technology (see figure 7(*c*)), unless excessive distortions of the cell body are accepted [18].

2.2. Microfabrication technology

MEMS technology development started a couple of decades ago with the anisotropic wet etching of silicon, at first mainly based on the microelectronics industry processes. Since then, inventions like DRIE (deep reactive ion etching) allowed creating three-dimensional structures in bulk substrates, mainly on silicon, with different shapes, high aspect ratios and typical dimensions and resolution below the micrometer scale. The advances in bonding techniques allowed creating more and more complex and ever smaller structures also in three dimensions.

One of the major advantages of this technology for producing alkali cells is the possibility of processing many samples in parallel at wafer level and the freedom in the shapes that can be given to even very small structures as they are defined by a photolithographic mask. Excellent reproducibility of the cell geometry can be obtained, which is of relevance for realistic simulations of the cell influence on, e.g., the electro-mechanical or thermal behaviour of MEMS devices using such cells. On the other hand, this technology requires highly specialized and expensive equipment. While the fabrication of a limited number of samples results in very high cost per chip, the technology allows reducing this cost when reaching high numbers of cells. By bonding several of these wafers together to form a hollow cell cavity, the obtained sidewalls have very little roughness and it is possible to obtain almost perfectly flat and polished window surfaces. Different bonding techniques have been demonstrated for hermetic sealing of the cells [10, 19–22], required to prevent oxidation of the alkali metals. Several alkali filling methods of atomic clocks cells were also reported [7, 9, 10, 21, 23] but the precise amount of alkali is often difficult to control. Working microfabricated cells were presented in the last few years and accelerated thermal aging tests were already performed [24] but only very few studies are reported on the long-term behaviour of micro-fabricated alkali cells over several months [6, 24].

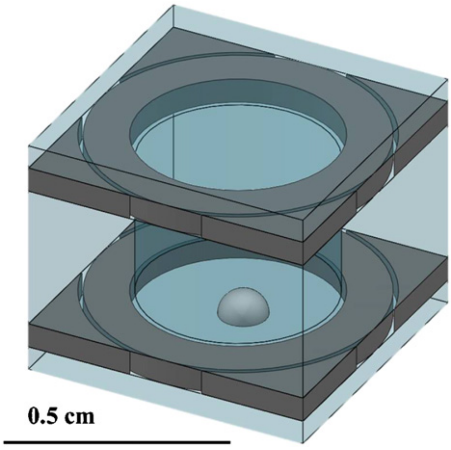

Figure 1. CAD image of the designed 4 mm thick vapour cell.

3. Vapour-cell design and fabrication process

3.1. Cell design

Our cell design is driven by the goal to sample more Rb atoms, and in a bigger cell than our previous 2 mm thick microfabricated cells developed for a small-scale atomic clock [16], in order to achieve a better signal for improved clock stability.

The designed chip is represented in figure 1. Its inner cylindrical cavity has dimensions of 4.0 mm diameter and 4.05 mm height; the outer footprint is 6×6 mm^2 and 5.05 mm outer height. These dimensions are much larger than any other previously reported microfabricated atomic vapour cell.

The cell is composed of a 3 mm thick core glass into which a through-hole is drilled, and to which are bonded two rims of 525 μm thick silicon on each side, creating a 4.05 mm long hollow cylindrical cavity.

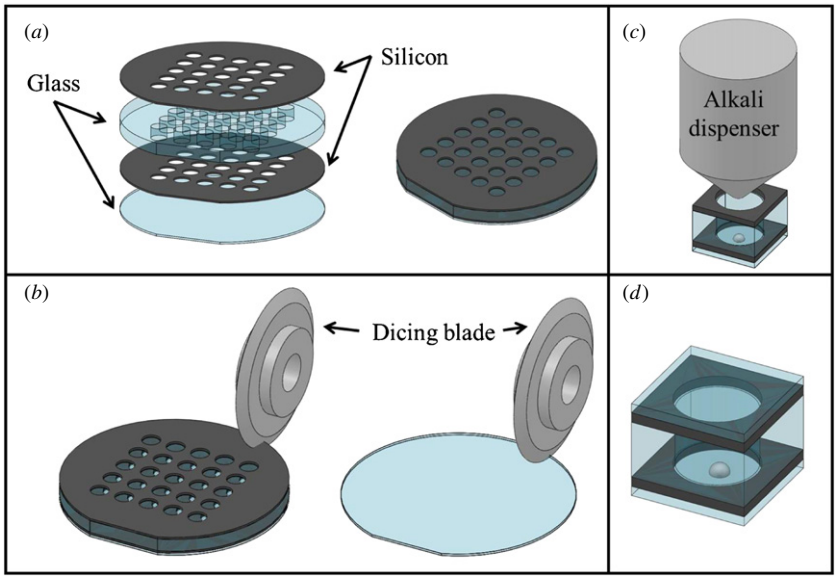

Figure 2. Fabrication procedure. (*a*) Patterning and cleaning two silicon wafers and one thick glass wafer. Bonding those together and to another unpatterned glass wafer, to obtain a stack with an array of cell preforms. (*b*) Dicing into single chips the obtained stack and another glass wafer. (*c*) Dispensing alkali in the preform of the obtained chip by atomic jet. (*d*) Bonding of a glass lid on top of the preform by anodic bonding.

The central cavity on the silicon wafer is etched with a diameter slightly larger than the one of the glass in order to obtain a 100 μm recess. Additionally, for symmetry reasons, not to get any problem with any electric and magnetic fields applied to the structure, a circular trench 100 μm wide is etched to obtain a rim of silicon. During wafer-level processing, these rims are maintained together by thin arms to the wafer frame that are later removed during the final dicing of the chip.

This cavity is closed on both sides with 500 μm thick glass lids to form the cell and contains a droplet of metallic Rb.

Note that this technology is not limited to the precise cell size described here and that it is possible to increase even further the thickness of the stack if required. Limits of the manufacturing technology are more linked to the anodic bonding equipment available than to the technology of anodic bonding.

3.2. Fabrication process

Multiple-stack anodic bonding of silicon and glass at wafer level has already been reported in the literature [25, 26]. It was shown that it is feasible to perform anodic bonding without electrically connecting directly the two substrates to be bonded. For high enough voltages, the electric field created through the entire stack of additional substrate layers is sufficient to obtain a stable and hermetic anodic bonding.

A schematic view of the process is shown in figure 2. Our approach is to start with a thick glass wafer in which through-holes are cut by mechanical drilling (currently up to 117 cells per 4 inch wafer). After cleaning the substrates, this glass wafer is anodically bonded to a first silicon wafer patterned by DRIE. The result obtained is bonded to a glass wafer to create the bottom windows of the cavities. This stack of three wafers is in turn bonded to a second, identical silicon wafer (also patterned by DRIE) on the other side of the thick glass substrate. These bonding steps are performed in a bonding machine (Bonder SB6 E, SUSS MicroTech) at 360 °C and up to 1200 V. The bonding voltage is applied once the temperature is stabilized and is stopped once the bonding current drops down to 5% of its maximal value. The measured curves of the first and last wafer-level bondings are shown in figure 3. These show that even if the voltage is higher (1200 V instead of 1000 V), the total amount of charges travelling (obtained by integrating the bonding current over time) is lower on the last wafer-level bonding step: during the first bonding step, a total electric charge of 1.94 C was measured for the first interface and only 0.45 C for the last one. The total amount of charges is in the expected range of a couple of mC cm^{--2} (depending on the process parameters and materials) [27, 28]. This difference can be attributed to the additional layers of the substrate present for the last bonding step and makes us expect this last bonding interface to be the weakest of all bonds. A photograph of a fully bonded wafer (diced on its centre) is shown in figure 4.

The obtained stack is then diced to obtain single-cell preforms, using a double-sided dicing process. The dicing is performed on both sides due to the large thickness of the structures (4550 μm). The alignment of the blade is performed on 50 μm wide dicing marks patterned on both silicon wafers. At the same time, a 500 μm thick glass wafer is diced into smaller pieces with the same lateral dimensions than the cavities (figure 2(*b*)). Note that this dicing of the wafer into single cells is performed at this moment only for development reasons. In future cell production, it will be more advantageous to perform dicing only after all cell preforms on the wafer are filled and sealed off in parallel, as described in the following.

The diced preforms are then filled with a droplet of alkali (figure 2(*c*)) and the glass lids are anodically bonded on top (figure 2(*d*)). The alkali dispensing technology used for this filling was previously presented in [16]. The method is based

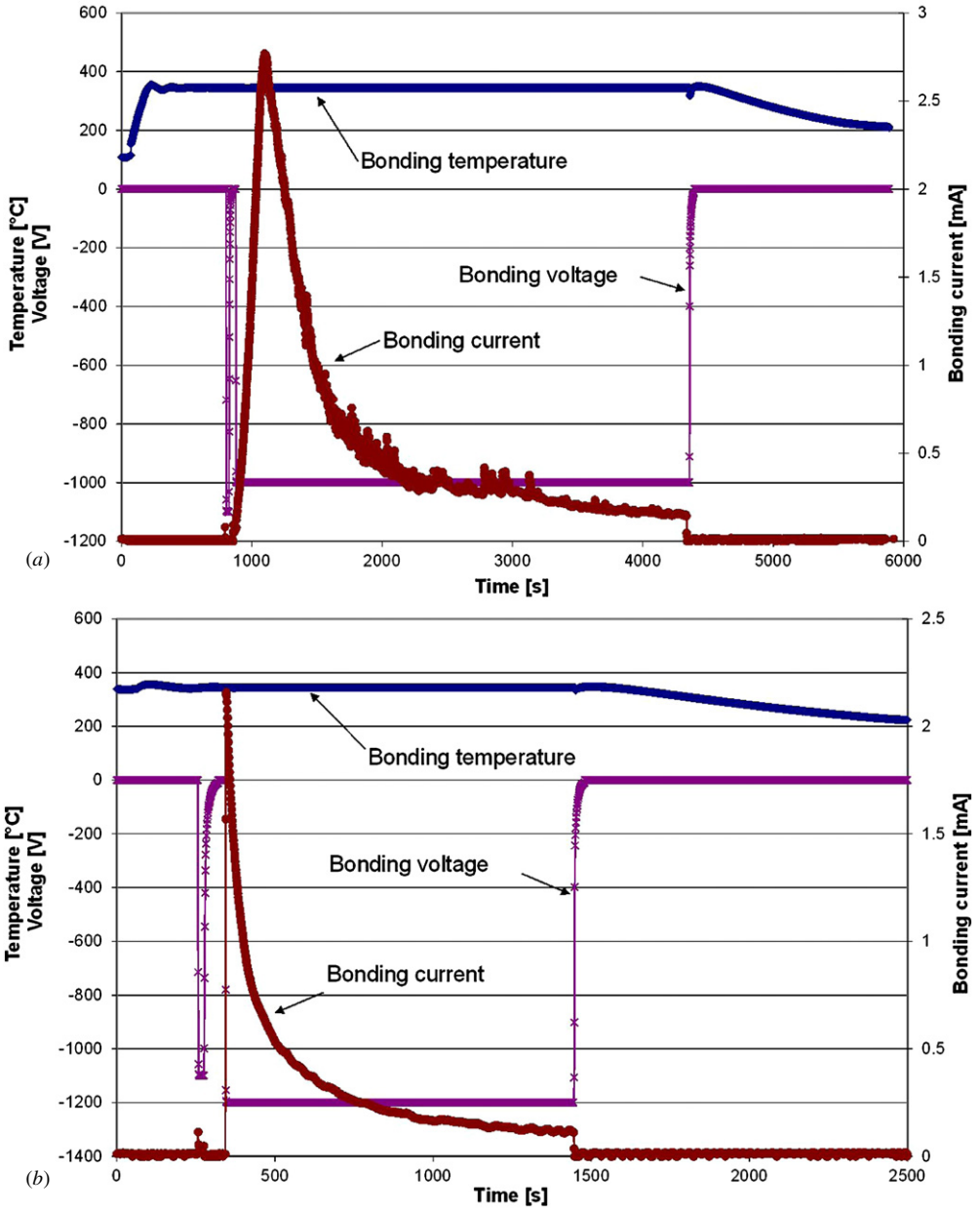

Figure 3. Bonding curves of some of the recorded parameters (bonding temperature, voltage applied and bonding current) for the first (*a*) and last (*b*) bonding steps performed to produce the cell preforms.

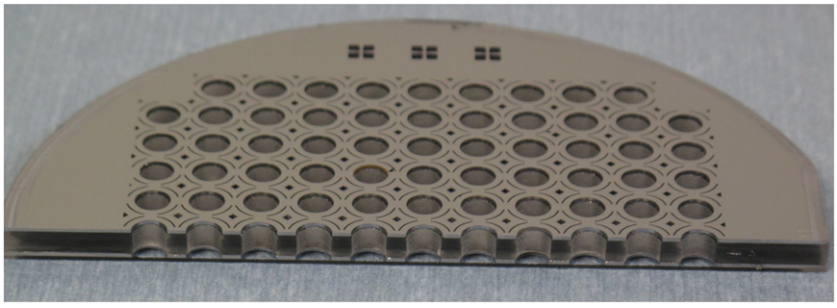

Figure 4. Photograph of a wafer (diced into two pieces) after the three bonding steps at wafer level.

on the condensation of alkali vapour—in our case, natural rubidium—produced by a commercially available dispenser from SAES Getters. After being degassed, the dispenser is selectively heated by applying a controlled current. Alkali vapour is released and condenses inside the cooled cell preform placed below the dispenser. The next step consists in moving a mobile trolley—on which the alkali-filled preform is placed—to the bonding position, controlling the chamber atmosphere

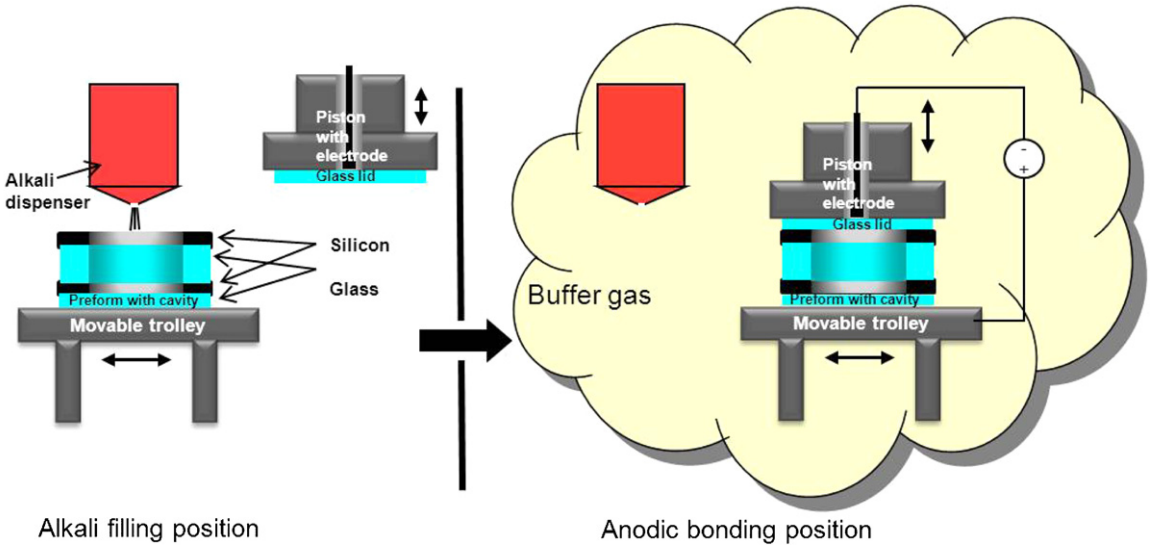

Figure 5. Schematic view of the dispensing and bonding procedure.

with buffer gas if needed, and moving the vertical piston to close the cell. To perform the bonding, the system is then heated up (max 300 °C) and a voltage is applied. A schematic view of the system is shown in figure 5.

When adding buffer gas in the cell, depending on the gas and its pressure, the lid bonding voltage has to be decreased in order to avoid discharges during the process. As reduced voltages cause longer bonding times, a two-step anodic bonding is carried out. A first bonding step is performed at lower voltage with the desired buffer gas pressure (typically a couple of tens of millibars) and then a second bonding step at higher voltage and higher gas pressure (∼500 mbar) is completed. Figure 6 shows the voltage applied, the temperature, the pressure and the measured current during this process step.

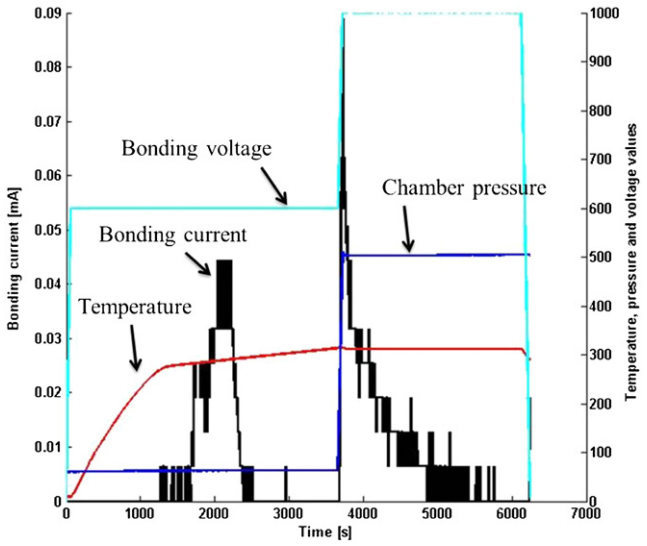

Figure 6. Bonding curve of the bonding current, temperature, pressure and voltage of the last two-step bonding process.

4. Fabrication and spectroscopy results

4.1. Fabricated cell

A cell fabricated according to the described process is shown in figures 7(a) and (*b*). Figure 7(*a*) shows a top view of the cell. A small metallic spot of metallic Rb is visible in the centre of the cavity. Figure 7(*b*) shows an isometric view of the device. A cylindrical vapour cell with the same inner cavity dimensions (4 mm diameter and 4 mm length) produced by conventional glass-blowing technology is depicted in figure 7(*c*). From these figures it is evident that the microfabrication method for these cells gives by far the better control of the cell geometry. Also note that the glass-blowing approach leaves a few mm long seal-off tube attached to the cell for cell filling and sealing (not visible in figure 7(*c*)), which can be cumbersome for integration of the cell into e.g. the clock application. This seal-off tube is not present in the microfabrication technique.

The bonding strengths of the different bonding steps were analysed by performing pull-tests on several cell samples. These experiments were carried out on eight fully fabricated chips (four bonding steps performed). Sample holders were glued on both sides to the 500 μm thick glass windows and pull-tests were performed on dedicated pull-test equipment (Model 3344, Instron). After breaking of the cell, it was optically inspected where (at or close to which bonding interface) the chip was broken. The number of broken chips at each interface was then reported in figure 8, from which one deduce that the two last bonding steps (and especially the last one) are weaker than the first ones. Our explanation is the presence of small voids in the bonding interfaces. This could explain the lower amount of charge and the weaker bond. These voids reduce the bonding area, resulting in a larger pull-test pressure on the bonded surface. Unfortunately, due to the thickness of the stack, these could not be visualized with an infrared camera. In spite of the presence of voids and the weaker bonding interfaces evidenced, the whole assembly is hermetic, proven by the absence of oxidation of Rb in the cavity. Alkali metals being very reactive with oxygen, in case of a leak, the entering air would create Rb oxide, which was not

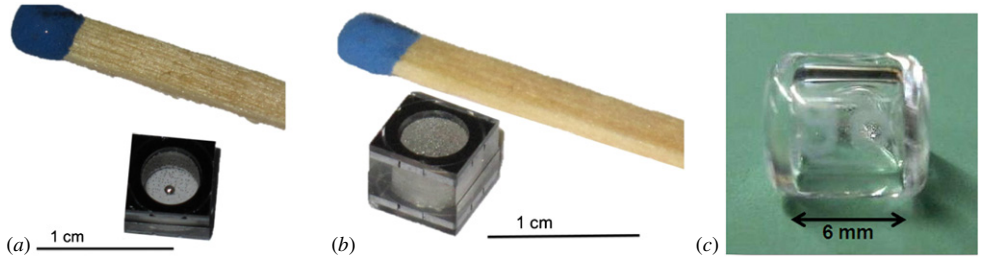

Figure 7. Pictures of the obtained cell. (*a*) Top view. A small spot of alkali metal can be seen in the cavity. (*b*) Isometric view. (*c*) Glass-blown vapour cell of the same dimensions; the deviations from the ideal cylindrical shape are clearly visible here.

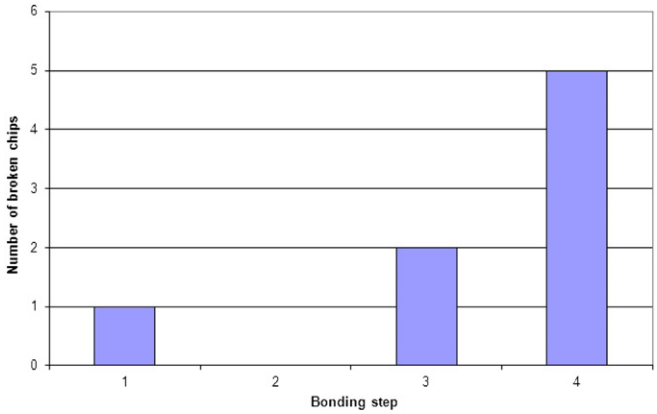

Figure 8. Number of chips broken on the interface of each anodic bonding step.

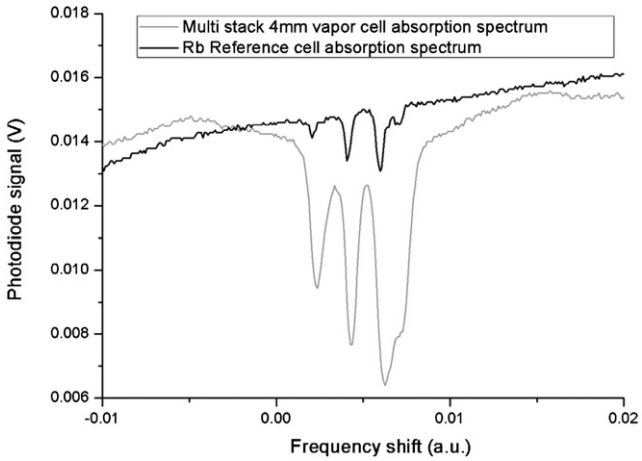

Figure 10. Absorption spectra of the 4 mm thick rubidium cell (grey) and the reference cell (black).

observed in the cavity. Another proof of hermeticity is given by the spectroscopic measurements performed, as described below. A strong increase of pressure inside the cell (due to a leak) would drastically broaden and flatten the optical and DR signals, which is not observed.

Preliminary tests to confirm the presence of Rb vapour in the cell were performed using optical absorption spectroscopy. Figure 9 shows the basic setup used to perform these measurements. The light generated by a VCSEL (vertical-cavity surface-emitting laser diode) is collimated and split into two beams. These two beams are redirected to photodiodes after passing through the heated microfabricated cell for the first one and through a macroscopic glass-blown Rb reference cell for the second beam. The VCSEL's light output wavelength is swept through the Rb D2 line (around 780 nm) using a sawtooth signal from an external function generator. By triggering the photodiode response with this signal gives the Rb absorption spectra of the measured samples.

The spectra of figure 10 show the expected Rb absorption spectrum, for a cell heated to about 100 °C. In this graph, the black line represents the absorption spectrum of the macroscopic reference cell, while the grey line corresponds to the absorption spectrum of the 4 mm thick microfabricated cell. The visible broadening of the latter absorption lines is due to the pressure of the buffer gas intentionally filled into the cell.

4.2. Observation of DR clock signals

We have experimentally evaluated the suitability of the cells for the observation of DR clock signals [1], i.e. of the

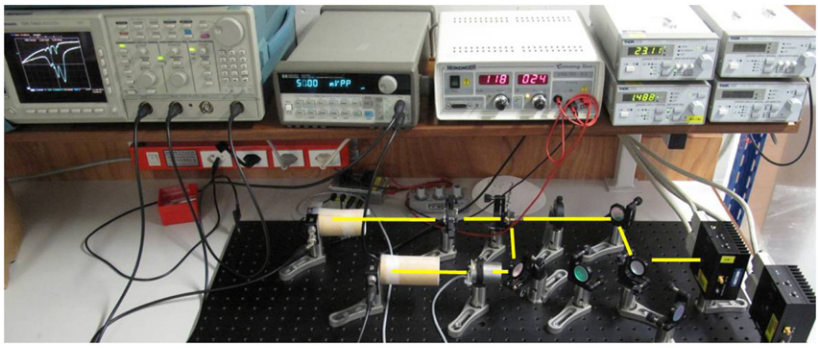

Figure 9. Picture of the absorption spectrum analysis setup. The light path (for Rb) is shown in yellow and the recorded spectrum can be seen on the oscilloscope (top left).

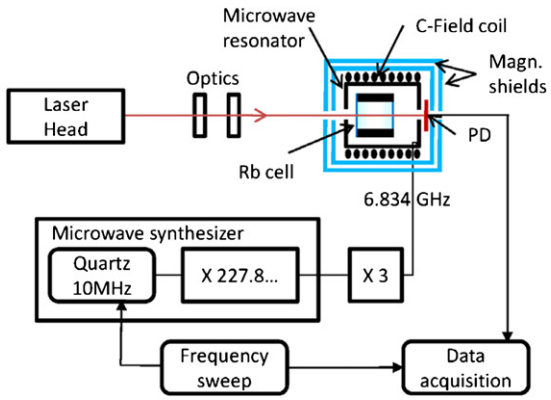

Figure 11. Experimental setup for DR spectroscopy.

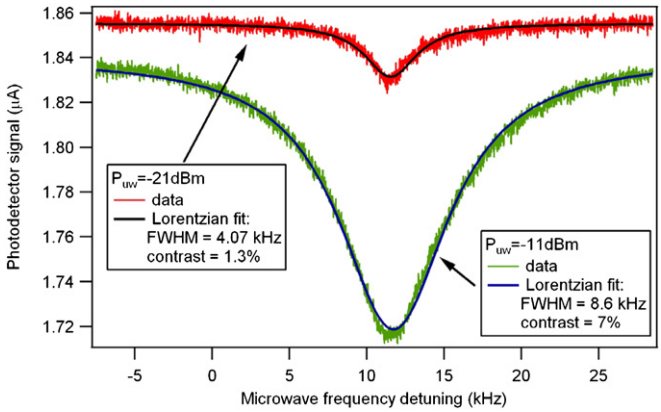

Figure 12. Examples of the DR signal observed at different microwave power P_{uw} coupled to the cavity, showing good contrast and narrow linewidths. For this measurement, the cell is heated up to 87 °C.

ground-state $|F = 1, m_F = 0\rangle \rightarrow |F = 2, m_F = 0\rangle$ microwave 'clock' transition in ^{87}Rb, as required for a Rb atomic clock [2].

The experimental setup used is sketched in figure 11. The cell is placed inside a compact magnetron-type microwave resonator [29] that is resonant with the clock transition at 6.834 GHz and assures the desired geometry of the microwave field. The microwave resonator and the cell are heated to 87 °C, in order to increase the density of the Rb vapour in the cell. A C-field coil applies a static magnetic field to split off the undesired Zeeman transitions, and a two-layer magnetic shield attenuates fluctuations of the external magnetic field. Laser light resonant with the Rb D2 line at 780 nm obtained from a compact, frequency-stabilized laser head [30] is used for optical pumping of the Rb atoms. The microwave frequency is generated from a commercial synthesizer whose $\approx$ 2.278 GHz output is multiplied to $\approx$ 6.834 GHz using a frequency tripler. Clock signals are recorded by sweeping the microwave frequency and recording the light intensity transmitted through the cell, detected on a Si photo-detector ($\approx$ 0.5 A W^{-1} efficiency).

Figure 12 gives examples of clock signals observed for microwave drive powers of −21 and −11 dBm coupled to the microwave resonator, showing contrasts of 1.3% and 7%, and linewidths of 4.7 and 8.6 kHz, respectively. These linewidths

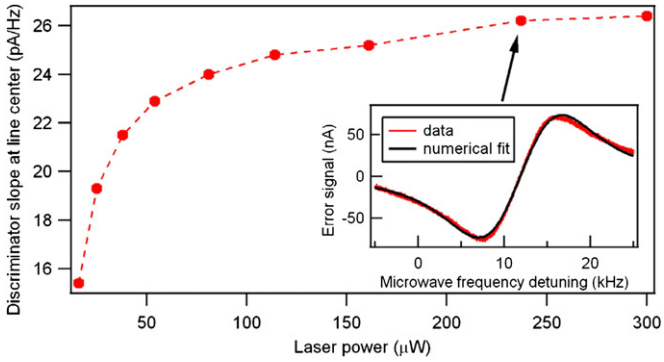

Figure 13. Discriminator slope as a function of laser power, scaled to the current of the Si photo-detector. The inset shows the error signal obtained by lock-in detection, at 237 μW of laser power (beam cross-section 0.25 mm^2).

are approximately two to four times higher than calculated from the cell geometry and gas content (see chapter 3.5.1 of [2]), due to power broadening by the laser and microwave radiation, and can still be optimized.

For operation of an atomic clock, the discriminator slope, i.e. slope at line centre obtained by frequency modulation of the microwave signal and lock-in detection (inset of figure 13), is of relevance [31]. Figure 13 shows the measured discriminator slope for our cell as a function of laser power. Combining these values with the typical detection noise on the level of $\approx$8 pA Hz$^{-1/2}$, we predict a clock stability of $\approx 3 \times 10^{-11}$ at 1 s of integration time. This stability compares well to the performance of commercial compact Rb atomic clocks.

5. Conclusion

We have presented the fabrication and evaluation of a new type of mm scale alkali cells using thick glass wafers, manufactured using microfabrication technology. Shear tests and optical spectroscopy measurements demonstrate stable and hermetic bonding of the cell. DR clock signals were measured and show that the clock signal obtained with our cells is compatible with a clock stability of about $3 \times 10^{-11}\ \tau^{-1/2}$.

The presented technology opens the perspective for massively parallel production of Rb vapour cells of dimensions of few millimetres by using MEMS/microfabrication technologies. These cells are of interest for use in novel compact or miniaturized atomic devices using small vapour cells, such as Rb atomic clocks, atomic magnetometers and gyroscopes.

Acknowledgments

This work was supported by the Swiss National Science Foundation (Sinergia grant CRSI20-122693/1). The authors would like to thank the CSEM microsystems division staff, Idonus Sarl and all the project partners for their contribution and help. LTF also acknowledges the European Space Agency and the Swiss State Secretariat for Education and Research—Space Division. We thank F Gruet, P Scherler and M Durrenberger (all LTF) for their experimental support.

References

[1] Camparo J 2007 The rubidium clock and basic research *Phys. Today* November 33–9

[2] Vanier J and Audoin C 1989 *The Quantum Physics of Atomic Frequency Standards* (Bristol: Hilger) chapter 7 pp 1257–363

[3] Knappe S 2008 MEMS atomic clocks *Compr. Microsyst.* **3** 571–612

[4] Riley W J 2008 *Handbook of Frequency Stability Analysis* (Boulder, CO: National Institute of Standards and Technology) NIST Special Publication 1065

[5] Kitching J, Knappe S and Hollberg L 2002 Miniature vapor-cell atomic-frequency references *Appl. Phys. Lett.* **81** 553–5

[6] Lutwak R *et al* 2007 The chip-scale atomic clock—prototype evaluation *Proc. 39th Annu. Precise Time and Time Interval (PTTI) Meeting (Long Beach, CA, 26–29 November 2007)* pp 269–90

[7] Hasegawa M *et al* 2011 Microfabrication of cesium vapor cells with buffer gas for MEMS atomic clocks *Sensors Actuators* A **167** 594–601

[8] DeNatale N F *et al* 2008 Compact, low-power chip-scale atomic clock *Proc. IEEE/ION PLANS (Monterey, CA, 6–8 May 2008)* pp 67–70

[9] Gong F, Jau Y-Y, Jensen K and Happer W 2006 Electrolytic fabrication of atomic clock cells *Rev. Sci. Instrum.* **77** 076101

[10] Liew L-A *et al* 2004 Microfabricated alkali atom vapor cells *Appl. Phys. Lett.* **84** 2694–6

[11] Lee C-H *et al* 2004 A batch fabricated rubidium–vapor resonance cell for chip-scale atomic clocks *Proc. Solid-State Sensors, Actuators and Microsystems Workshop (Hilton Head Island, SC, 6–10 June 2004)* pp 23–6

[12] Lutwak R, Emmons D, Riley W and Garvey R M 2002 The chip-scale atomic clock—coherent population trapping vs conventional interrogation *Proc. 34th Annu. Precise Time and Time Interval (PTTI) Meeting (Reston, VA, 3–5 December 2002)* pp 539–50

[13] Haesler J, Bennès J and Lecomte S 2010 Advances in the development of an extra small atomic reference (XSAR) *Proc. European Frequency and Time Forum (EFTF) (Noordwijk, NL, 13–15 April 2010)* p 127

[14] Schori C, Mileti G, Leuenbeger B and Rochat P 2010 CPT atomic clock based on rubidium 85 *Proc. European Frequency and Time Forum (EFTF) (Noordwijk, NL, 13–15 April 2010)* p 125

[15] Deng J, Vlitas P, Taylor D, Perletz L and Lutwak R 2008 A commercial CPT rubidium clock *Proc. European Frequency and Time Forum (EFTF) (Toulouse, FR, 22–25 April 2008)* pp E3B01–0099

[16] Pellaton M, Pétremand Y, Affolderbach C, Mileti G and de Rooij N F 2011 Laser-pumped double-resonance clock using a micro-fabricated cell *Proc. IEEE Int. Frequency control Symp. jointly with the European Frequency and Time Forum (IFCS-EFTF) (San Francisco, CA, 1–5 May 2011)* pp 604–6

[17] Starr F 1998 *A Resource for Glass* (Corning, NY: The Corning Museum of Glass Education Dept))

[18] Knappe S, Velichansky V, Robinson H G, Liew L, Moreland J, Kitching J and Hollberg L 2003 Atomic vapour cells for miniature frequency references *Proc. IEEE Int. Frequency Control Symp. and PDA Exhibition Jointly with the European Frequency and Time Forum (IFCS-EFTF) (Tampa, FL, 2003)* pp 31–2

[19] Douahi A, Nieradko L, Beugnot J C, Dziuban J, Maillote H, Guerandel S, Moraja M, Gorecki C and Giordano V 2007 Vapour microcell for chip scale atomic frequency standard *Electron. Lett.* **43** 279–80

[20] Tsujimoto K, Hirai Y, Sugano K, Tsuchiya T and Tabata O 2011 Sacrificial microchannel sealing by glass-frit reflow for chip scale atomic magnetometer *Proc. IEEE 24th Int. Conf. on Micro Electro Mechanical Systems (MEMS2011) (Cancun, Mexico, 23–27 January 2011)* pp 368–71

[21] Vecchio F, Venkatraman V, Shea H, Maeder T and Ryser P 2011 Dispensing and hermetic sealing Rb in a miniature reference cell *Sensors Actuators* A **172** 330–5

[22] Pétremand Y *et al* 2010 Low temperature indium-based sealing of microfabricated alkali cells for chip scale atomic clocks *Proc. European Frequency and Time Forum (EFTF) (Noordwijk, NL, 13–15 April 2010)* p 119

[23] Liew A-L, Moreland J and Gerginov V 2007 Wafer-level filling of microfabricated atomic vapor cells based on thin-film deposition and photolysis of cesium azide *Appl. Phys Lett.* **90** 114106

[24] Hasegawa M *et al* 2011 Microfabrication and thermal behavior of miniature cesium-vapor cells for atomic clock operations *Proc. IEEE 24th Int. Conf. on Micro Electro Mechanical Systems (MEMS2011) (Cancun, Mexico, 23–27 January 2011)* pp 712–5

[25] Puers B and Lapadatu D 1994 Extremely miniaturized capacitive movement sensors using new suspension systems *Sensors Actuators* A **41** 129–35

[26] Lee K Y, Rishton S A and Chang T H P 1994 High aspect ratio aligned multilayer microstructure fabrication *J. Vac. Sci. Technol.* B **12** 3425

[27] Albaugh K B and Rasmussen D H 1992 Rate processes during anodic bonding *J. Am. Ceram. Soc.* **75** 2644–8

[28] Djuban J 2006 *Bonding in Microsystem Technology* (Berlin: Springer) chapter 4

[29] Affolderbach C, Droz F and Mileti G 2006 Experimental demonstration of a compact and high-performance laser-pumped rubidium gas-cell atomic frequency standard *IEEE Trans. Instrum. Meas.* **55** 429–35

[30] Affolderbach C and Mileti G 2005 A compact laser head with high-frequency stability for Rb atomic clocks and optical instrumentation *Rev. Sci.Instrum.* **76** 073108

[31] Bandi T, Affolderbach C, Calosso C E and Mileti G 2011 High-performance laser-pumped rubidium frequency standard for satellite navigation *Electron. Lett.* **47** 698–9